



J-resistance curves for Inconel 690 and Incoloy 800 nuclear steam generator tubes at room temperature and at 300 °C



Marcos A. Bergant^{a,*}, Alejandro A. Yawny^b, Juan E. Perez Ipiña^c

^a Gerencia CAREM, Centro Atómico Bariloche (CNEA), Av. Bustillo 9500, San Carlos de Bariloche 8400, Argentina

^b División Física de Metales, Centro Atómico Bariloche (CNEA) / CONICET, Av. Bustillo 9500, San Carlos de Bariloche 8400, Argentina

^c Grupo Mecánica de Fractura, Universidad Nacional del Comahue / CONICET, Buenos Aires 1400, Neuquén 8300, Argentina

HIGHLIGHTS

- Non-standard fracture specimens were obtained from nuclear steam generator tubes.
- Specimens with circumferential and longitudinal through-wall cracks were used.
- Inconel 690 and Incoloy 800 steam generator tubes were tested at 24 and 300 °C.
- Fracture toughness for circumferential cracks was higher than for longitudinal cracks.
- Incoloy 800 showed higher fracture toughness than Inconel 690 steam generator tubes.

ARTICLE INFO

Article history:

Received 2 September 2016
Received in revised form
18 January 2017
Accepted 23 January 2017
Available online 24 January 2017

Keywords:

Fracture toughness
J-resistance curve
Non-standard specimens
Steam generator tubes
Inconel 690
Incoloy 800

ABSTRACT

The structural integrity of steam generator tubes is a relevant issue concerning nuclear plant safety. In the present work, *J*-resistance curves of Inconel 690 and Incoloy 800 nuclear steam generator tubes with circumferential and longitudinal through wall cracks were obtained at room temperature and 300 °C using recently developed non-standard specimens' geometries. It was found that Incoloy 800 tubes exhibited higher *J*-resistance curves than Inconel 690 for both crack orientations. For both materials, circumferential cracks resulted into higher fracture resistance than longitudinal cracks, indicating a certain degree of texture anisotropy introduced by the tube fabrication process. From a practical point of view, temperature effects have found to be negligible in all cases. The results obtained in the present work provide a general framework for further application to structural integrity assessments of cracked tubes in a variety of nuclear steam generator designs.

© 2017 Elsevier B.V. All rights reserved.

1. Introduction

Steam generators (SGs) are large heat exchangers that use the heat produced in a nuclear reactor core to convert liquid water into steam. SGs consist in a bundle of thousands of thin-walled tubes arranged inside a pressure vessel. The steam generator tubes (SGTs) act as the physical barrier between the primary and secondary coolant circuits of a nuclear power plant, representing up to 60% of the total primary pressure retaining boundary [1]. In case of rupture of the tube walls, the primary water at higher pressure will

leak to the secondary circuit and a potential release of radioactivity may occur. Therefore, the structural integrity of SGTs is a relevant issue concerning the plant safety.

The nuclear industry has developed acceptance criteria for SGTs defects in order to ensure a low probability of spontaneous failures during normal or accident conditions. Former criteria were based on Limit Load Analyses assuming that plastic collapse is the prevailing failure mode due to the inherent high toughness of SGTs made of austenitic materials [1–5]. However, this assumption has not been properly validated mainly due to the lack of appropriate fracture toughness data characterizing SGTs materials. On the other hand, the experience has also shown that Limit Load criteria result excessively conservative for crack like defects [1]. To overcome this limitation, alternative criteria based on fracture mechanics methodologies have been proposed by different authors [6–13] and

* Corresponding author.

E-mail addresses: marcos.bergant@cab.cnea.gov.ar (M.A. Bergant), yawny@cab.cnea.gov.ar (A.A. Yawny), juan.perezzipina@fain.uncoma.edu.ar (J.E. Perez Ipiña).

more recently by Bergant and co-workers [14,15]. For their application however, knowledge of fracture properties of actual SGTs at typical operating temperatures is required.

In this context, a research effort is being conducted in the last years by the present authors in order to obtain specific and appropriate experimental data of fracture toughness of SGTs [16–18]. In effect, only few references are available in the open literature [12,16,18,19]. This is probably related with the impossibility of using standardized specimens considering the small dimensions of the SGTs and the high ductility of the associated materials.

In order to overcome these limitations, different novel specimens' geometries obtainable from SGTs were proposed in a previous work [17]. Due to their in-service significance [20], specimens with circumferential and longitudinal through-wall cracks (TWCs) were considered. Also high and low constraint testing configurations, i.e., bending and tensile prevailing loadings, respectively, have been analyzed. In order to estimate J values for J -resistance curve construction, the applicability of the η -factor method for the specific geometries was studied numerically [16,17]. In a subsequent work Bergant et al. [18] presented the experimental results of a testing research with the proposed specimens fabricated from Incoloy 800 SGTs. Fracture tests were performed at room temperature. That paper also included the description of the pre-cracking procedure and the implementation of an optical technique and the normalization method for determining the crack length during stable crack growth. The later was intended for high temperature tests where the optical devices cannot be used.

The present work represents a natural extension of the just mentioned previous works [16–18]. Two classical SGTs materials, i.e., Inconel 690 and Incoloy 800, were now studied considering that almost all new Western SGs are constructed with them. This is due to their excellent corrosion resistance in the particular environment of nuclear SGs. Inconel 690 is a Ni-based high Cr alloy developed to improve the resistance to stress corrosion cracking (SCC) of Inconel 600 SGTs. Nowadays, Inconel 690 replaced Inconel 600 for SGTs in new SGs. On the other hand, Incoloy 800 is a Fe-based high Cr-Ni alloy that has been used for SGTs for more than 30 years, primarily in CANDU reactors and in German technology reactors.

Some of the specimens with circumferential and longitudinal TWCs proposed in previous works [17,18] were used in the present study. In order to evaluate the possible effect of the operating temperature on toughness properties, fracture testing was performed at room temperature and 300 °C. In this way, J -resistance curves and fracture toughness properties needed for a proper assessment of the structural integrity of SGTs at operating conditions are reported and compared with the scarce number of results available in the literature.

2. Experimental details

2.1. Materials

Fracture specimens were fabricated from austenitic alloys Inconel 690 thermally treated (UNS N06690) and Incoloy 800 (UNS N08800) SGTs with 15.88 mm external diameter and 0.97 and 1.13 mm wall thickness, respectively. Chemical compositions are given in Table 1 and were provided by the tubes' manufacturer (FAE SA, Ezeiza, Argentina).

Because of its importance for further analysis, the typical fabrication route of SGTs is briefly reviewed in what follows. The manufacture of SGTs starts with a hot extrusion of casted ingots, followed by cold pilgrip-process rolling stages with intermediate annealing treatments. These heat treatments promote the

Table 1

Chemical compositions of Inconel 690 and Incoloy 800 SGTs.

Inconel 690 (wt %)	Incoloy 800 (wt %)
Ni: 61	Ni: 33
Cr: 29	Cr: 21.6
Fe: 8.95	Fe: 42.2
C: 0.022	C: 0.017
Si: 0.02	Si: 0.54
Mn: 0.01	Mn: 0.55
Co: 0.03	Co: < 0.015
S: < 0.001	S: 0.003
P: < 0.005	P: < 0.01
N: 0.017	N: 0.008
Al: 0.23	Al: 0.29
B: < 0.001	Cu: 0.09
Ti: 0.28	Ti: 0.41
Mo: 0.05	Ti/C: 24
Nb: 0.08	Ti/(C + N): 17

recrystallization and carbide dissolution. The total thickness reduction ranges between 70 and 80% after three rolling stages. After the last reduction, a final recrystallization step is applied. In the particular case of Inconel 690 SGTs, an additional thermal treatment for carbide precipitation at grain boundaries is performed. Finally, the tubes are straightened by rollers that introduce a certain amount of plastic deformation increasing the material's resistance.

Fig. 1 shows micrographs of both alloys. The grain sizes are ASTM 6 and ASTM 8 (i.e., average diameters of 45 and 22 μm) for Inconel 690 and Incoloy 800, respectively. The finer grain size for Incoloy 800 SGT is due to the lower annealing temperature used, i.e., 960 °C instead of the 1070 °C used for Inconel 690. Due to the final annealing performed at high temperature, the microstructure is completely recrystallized with no evidence of deformed grains.

2.2. Tensile testing

Tensile data of actual SGTs was required for different purposes throughout the research. For instance, true stress vs. strain curves were used in the numerical simulation of fracture tests in order to estimate η -factors [16,17] and plastic collapse loads presented in section 4.3. Also the flow stress σ_f has been calculated from tensile properties, see section 4.3.

Uniaxial tensile tests were performed by loading the specimens under displacement control using servo-hydraulic testing machines MTS 810 and MTS Landmark, following the testing procedure recommended in ASTM A370-12 [21] for tubular products. The nominal strain rate adopted was 4.10^{-4} s^{-1} . Tests were performed in air at room temperature, i.e., 24 °C, and at 300 °C using the environmental chamber MTS 651. MTS and Epsilon extensometers were used for tensile tests at 24 °C and at 300 °C, respectively.

2.3. Fracture specimens

Based on the conclusions of a recent study [18], the specimen geometries described in what follows have been selected in the present work for J -resistance curve determination. The specimen nomenclature introduced in Refs. [17,18] is maintained here.

In the case of circumferential TWCs, tubular specimens denoted as T1 in Fig. 2(a) were considered. These specimens were either loaded in tension, specimen T1(T) in Fig. 2(b), or under four point bending conditions, specimen T1(B) in Fig. 2(b). Tubular specimens with two symmetric circumferential TWCs under tensile loading, i.e., T2(T) specimens, have been also analyzed in Ref. [18] but they were not considered in the present study due to the unlikelihood of their occurrence. For T1 specimens, a and W are the half crack

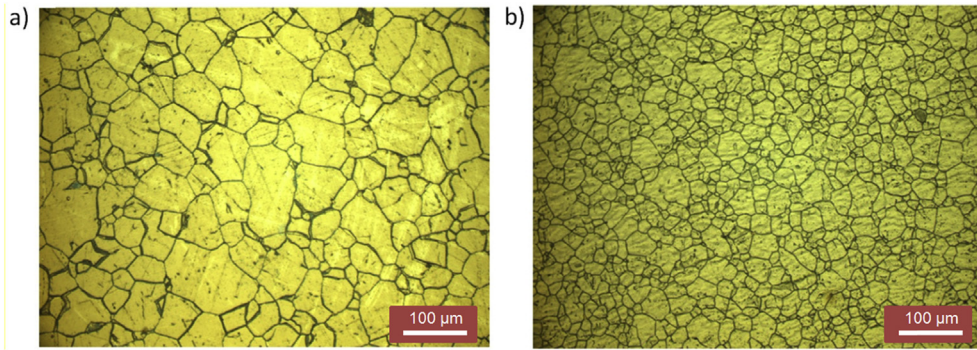


Fig. 1. Microstructures of (a) Inconel 690 and (b) Incoloy 800 SGTs (light microscope).

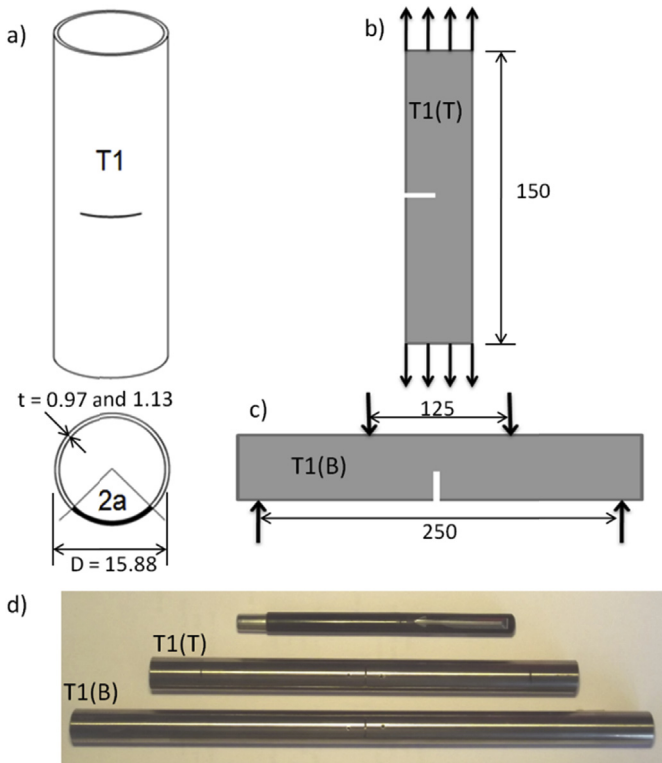


Fig. 2. Fracture specimens with circumferential TWCs: (a) representative tubular specimen with a single TWC, (b) T1(T) tensile specimen, (c) T1(B) bending specimen and (d) image of actual T1 type of specimens. Dimensions in mm.

length and the half mean perimeter of the tube, respectively.

The use of tensile and bending loadings aims assessing the effect of the degree of constraint level on the J -resistance curves. This is an important aspect that was considered in Bergant et al. [17,18] where the results indicated that tensile loading promotes lower constraint conditions than bending stresses, which in turns results in higher toughness properties.

In the case of longitudinal TWCs, the specimens illustrated in Fig. 3 have been adopted. In order to get symmetric loading conditions, specimens were fabricated by welding two half-specimens following the procedure detailed in Refs. [17,18]. In this case, manufacturing of the individual hemi-specimens was performed preserving a central circumference arc of the tube without plastic deformation. Thus, the original thermomechanical state of the SGTs was maintained in the region where the extension of longitudinal crack will take place. The specimens are referred to as C(T) and

SE(T) by analogy with the compact tension and single-edge-notched tension specimens, Fig. 3(a) and (b), respectively. Both type of specimens are designated with an additional “O” letter when the inner diameters of the two hemi-specimens were bonded facing each other. In case the hemi-specimens were bonded with the outer tube diameter in contact, they are designated by an additional “X” letter. The last condition was thought in order to prevent buckling of the remaining ligament in compression. As discussed in Bergant et al. [18], both configurations “O” or “X” gave J -resistance curves essentially equivalent as long as the a/W ratio is the same, and due to this they were used interchangeably in the present work.

It can be observed that C(T) and SE(T) specimens only differ in the position of the loading hole, Fig. 3(c) and (d). With the C(T) specimens it was intended to introduce predominantly bending stresses while with the SE(T) configuration, tensile loadings are promoted by applying the load through the hole located in the middle of the width W , i.e., $a/W \sim 0.5$. Therefore, the C(T) and SE(T) specimens can be respectively considered as higher and lower constraint longitudinal TWC specimens according to what explained in a previous paragraph.

The holes at the right of the SE(T) specimens illustrated in Fig. 3 were used for fatigue pre-cracking which was shown to result in more straight crack fronts when using a C(T) configuration in the procedure [18].

Along the present research, $a/W \sim 0.5$ was maintained for all specimens. In doing that, the degree of constraint is only related with the type of loading used. Thus, the effects of the degree of constraint associated with the in-plane dimensions of the specimens were not investigated here.

In all cases, for both circumferential and longitudinal TWCs, the specimens were notched using electrical discharge machining. Prior to fracture testing, the notched specimens were fatigue pre-cracked under load control up to an extension of approximately 1.3 mm, as explained in Ref. [18].

2.4. Fracture testing

All the fracture tests were performed by loading the specimens under displacement control using the servo-hydraulic testing machines. The displacement rate was maintained between 1 and 3 mm/min. Fig. 4 shows the testing arrangements used. The applied load P and the load-line displacement LLD were obtained from the testing machine. As showed in Bergant et al. [18], using P vs. LLD or P vs. $CMOD$ records lead to the same J -integral values. The first option was adopted in this work as the $CMOD$ acquisition at high temperature with conventional instrumentation is impractical.

Fracture testing was performed in air at room temperature,

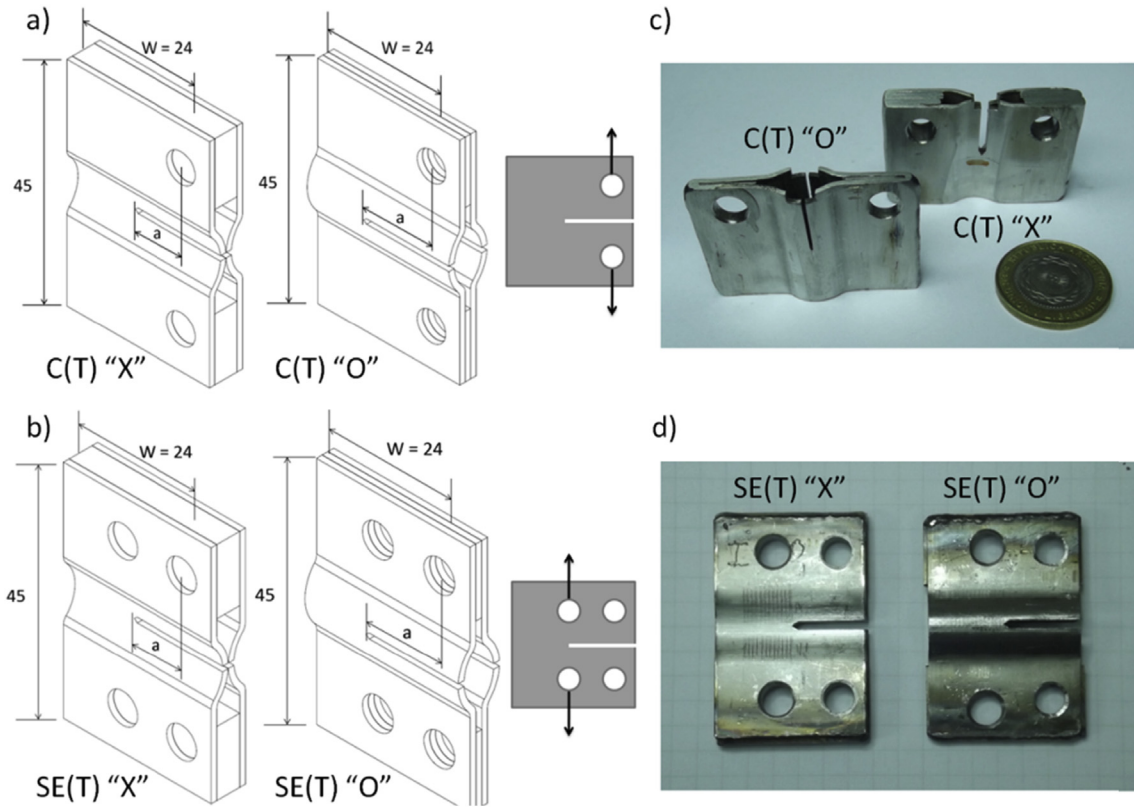


Fig. 3. Fracture specimens with longitudinal TWCs: (a) C(T) type specimens, (b) SE(T) type specimens, (c) and (d) images of actual specimens. Dimensions in mm.

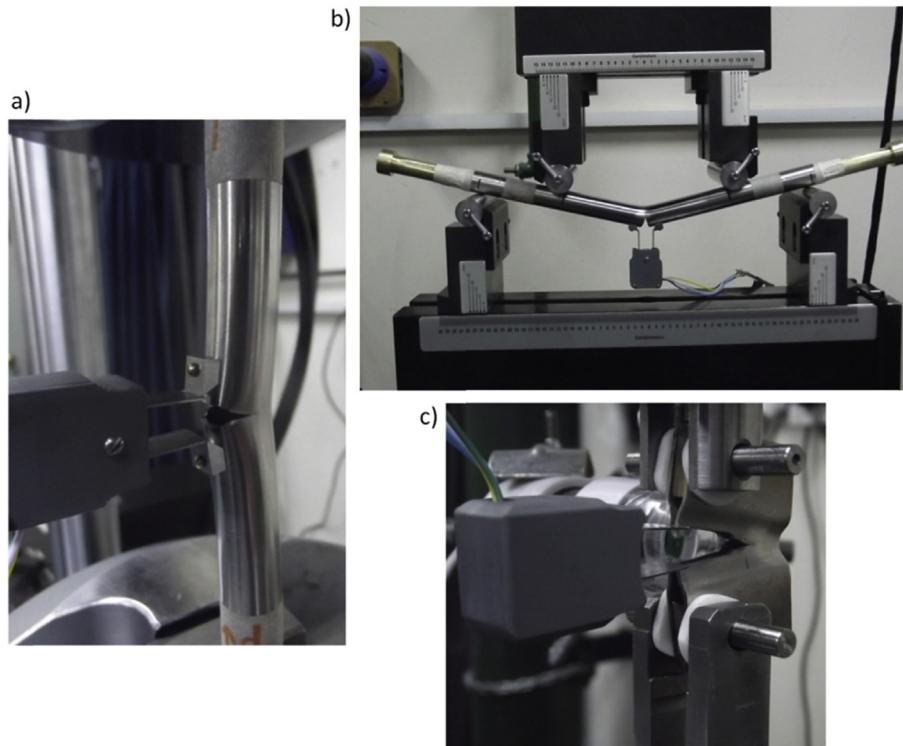


Fig. 4. Testing arrangements for tests performed at room temperature: (a) T1(T), (b) T1(B) and (c) C(T) "X" specimens. Clip gages were not used at 300 °C.

24 °C, and at 300 °C. A type-K thermocouple in contact with the specimen was used to register the temperature. In the tests

performed at 300 °C, a minimum of 30 min was used for temperature homogenization before testing. Temperature was controlled

within ± 3 °C along a test.

The stable crack growth Δa occurring during the fracture test was determined using the normalization method described in Bergant et al. [18]. As this method gives a continuous estimation of the crack length from the P vs. LLD record, the J -resistance curves could be presented as continuous lines. The maximum crack growth extension Δa_{max} was limited to 3 mm.

2.5. Estimation of J -resistance curves: the η -factor method

In order to estimate J values for J -resistance curve construction, the applicability of the η -factor method for the specific geometries here considered was demonstrated in Refs. [16,17]. Due to their significance in the context of the present work, some details are briefly reviewed in what follows.

The J -integral is usually expressed in a splitted elastic and plastic contribution [22]:

$$J = J_{el} + J_{pl} = \frac{K_I^2}{E/(1-\nu^2)} + J_{pl} \quad (1)$$

Here K_I is the Mode I linear elastic stress intensity factor, E is the Young's elastic modulus and ν is the Poisson's ratio. Under certain conditions, the plastic component J_{pl} can be related to the plastic work area U_{pl} under the P vs. LLD curve [17] in the following manner:

$$J_{pl} = -\frac{1}{B} \frac{dU_{pl}}{da} = \eta \frac{U_{pl}}{Bb} \quad (2)$$

where B is the specimen net section thickness, b the uncracked ligament length and η a calibration factor. The η -factor is a non-dimensional parameter which is assumed to depend on the flawed geometry and loading type (e.g., bending or tension) but independent of the loading magnitude P .

In a previous research, the values of the η -factors for some of the specimens presented in Figs. 2 and 3 with ratios a/W between 0.4 and 0.7 were estimated using the finite element method in order to simulate the fracture tests [17]. Using the same numerical procedure, the η -factors for SE(T) specimens were also obtained [23]. Fig. 5 summarizes the η -factors values as a function of a/W for the specimens used in this work. It should be noted that the η -factors were estimated for specimens made of Incoloy 800 SGTs, i.e., with wall thickness of 1.13 mm. Also, the stress vs. strain curve at room temperature for this material was used in the numerical models [17]. Simulations using stress vs. strain curves of Inconel 690 SGTs at room temperature and 0.97 mm of wall thickness showed

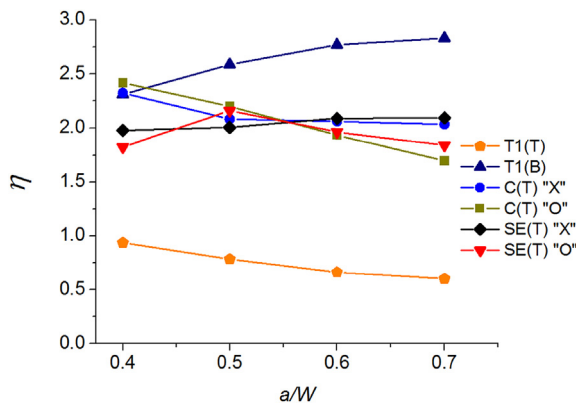


Fig. 5. η -factors for fracture specimens.

differences around 3% in the η -factors values regarding the results in Bergant et al. [17]. Therefore, it was assumed that the η -factors presented in Fig. 5 can be applied to specimens for both materials and for high temperature tests.

It is worth emphasizing here that the η -factors and J -resistance curves presented are strictly valid for the materials, specimens and SGTs geometries used in this work. Some validity limits upon which the J -integral derivation was based are not fulfilled, e.g., the thin wall thicknesses of SGTs. Therefore, the straight transferability of the results to other tube geometries must be prevented. The fracture toughness values reported here should be considered specific of the SGT material and geometry studied and not considered as an intrinsic material property [17,18].

Eq. (2) is valid for stationary, i.e., non-growing cracks, in which the non-linearity between the P vs. LLD behavior is due to plastic deformation only. When there is stable crack growth during the test, a new contribution to the non-linearity appears and the J -integral value must be corrected [24]. The J -resistance curves presented in what follows were corrected for crack growth using the procedure given in ASTM E1820-15 [25], as discussed in Bergant et al. [18]. Due to the small crack length growth achieved during fracture tests, the corrections were small.

3. Experimental results

3.1. Tensile testing

Fig. 6 presents the experimental stress vs. strain curves (true values) while Table 2 summarizes the derived basic mechanical properties. The curves corresponding to room temperature are represented up to maximum load, i.e., in the uniform deformation region. In the experiments performed at 300 °C the axial load was limited to a maximum of 25 kN due to the capacity of the gripping system employed. In these cases, maximum load could not be reached and ultimate tensile strengths σ_u values reported in ASME II Part D [26] for both material specifications were included in Table 2. Also the Young's elastic moduli E from ASME II Part D [26] were incorporated in Table 2, coinciding closely with the measured values.

3.2. J -resistance curves for circumferential TWCs

Figs. 7 and 8 present the J -resistance curves obtained at 24 °C and at 300 °C using specimens with circumferential TWCs

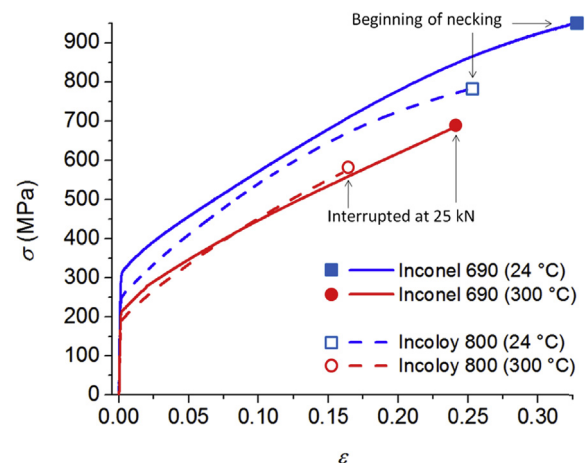


Fig. 6. Stress-strain curves (true values) corresponding to uniaxial tensile tests at 24 °C and at 300 °C for Inconel 690 and Incoloy 800 SGTs.

Table 2
Summary of basic mechanical properties for Inconel 690 and Incoloy 800 SGTs.

Properties	Inconel 690		Incoloy 800	
	24 °C	300 °C	24 °C	300 °C
Elastic modulus, E (GPa)	208 ^a	193 ^a	196 ^a	182 ^a
Yield strength, σ_{ys} (MPa)	320	218	260	198
Ultimate tensile strength, σ_u (MPa)	686	554 ^a	610	514 ^a

^a Values obtained from ASME II Part D [26].

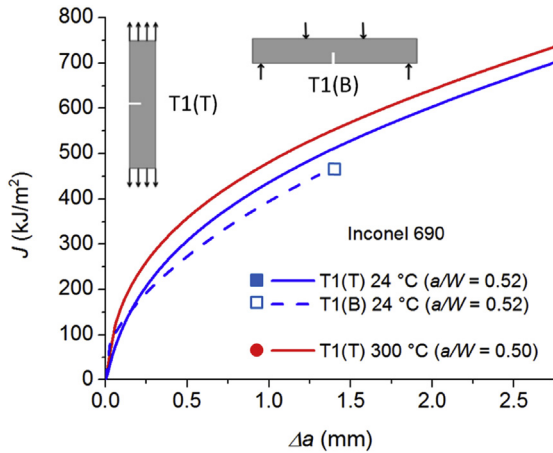


Fig. 7. J -resistance curves for circumferential TWCs in Inconel 690 SGTs.

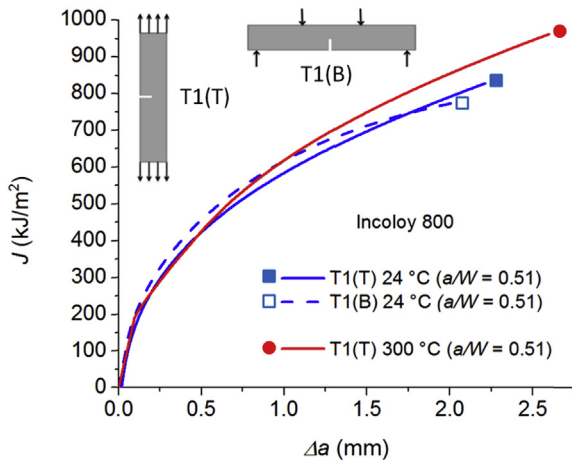


Fig. 8. J -resistance curves for circumferential TWCs in Incoloy 800 SGTs.

fabricated from Inconel 690 and Incoloy 800 SGTs, respectively. It can be seen that for both materials, the curves obtained with T1(T) and T1(B) specimens are similar for $a/W \sim 0.5$ at 24 °C. Only T1(T) specimens were used at 300 °C because their configuration is easier to test. However, the results show that the effect of temperature on the curves is reduced for both alloys.

3.3. J -resistance curves for longitudinal TWCs

Figs. 9 and 10 show the J -resistance curves for specimens with longitudinal TWCs tested at 24 °C and at 300 °C. It can be observed that for both materials, the SE(T) specimens gave slightly higher curves than C(T) specimens for $a/W \sim 0.5$. For both materials and specimen's geometries, the J -resistance curves at 300 °C presented

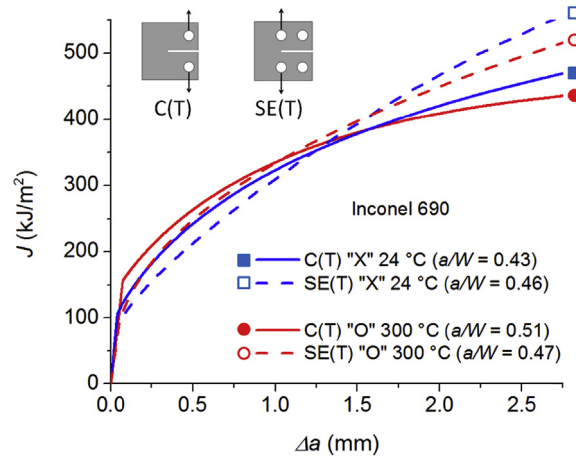


Fig. 9. J -resistance curves for longitudinal TWCs in Inconel 690 SGTs.

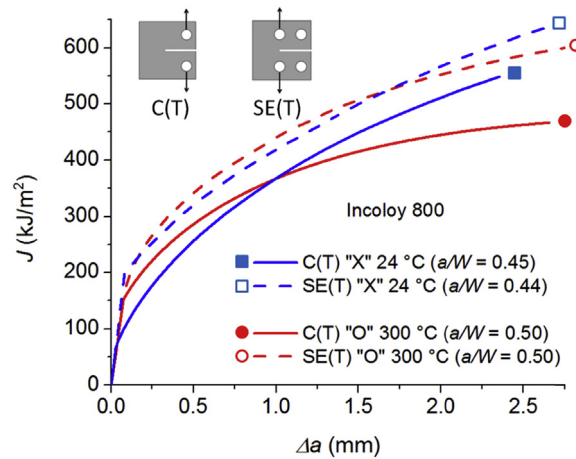


Fig. 10. J -resistance curves for longitudinal TWCs in Incoloy 800 SGTs.

a lower tearing modulus than the curves at room temperature. Despite this, the temperature effect is reduced from a practical point of view.

It should be remarked here that “X” and “O” configurations were used at 24 °C and at 300 °C, respectively. However, as mentioned before, both configurations gave almost identical J -resistance curves for the same testing conditions, i.e., SGT material, temperature and $a/W \sim 0.5$ [18], and therefore the results of both configurations can be compared among them.

4. Discussion

4.1. Temperature effects

As can be seen in Fig. 6, tensile properties of both SGTs studied here present a decrease in strength between 24 °C and 300 °C, as expected. For instance, the reduction in the measured yield strength σ_{ys} was about 38 and 27% for Inconel 690 and Incoloy 800, respectively.

On the other hand, another important observation from a practical point of view is the weak dependence of the J -resistance curves with the temperature observed in both materials for both circumferential and longitudinal TWCs. This fact will allow the use of room temperature testing in order to estimate the fracture properties of the SGTs under study. This option may simplify many

practical aspects related with the tests. For instance, the *CMOD* can be recorded with conventional clip gages and the *J*-integral may be estimated from *P* vs. *CMOD* records. This will be useful in the case where shallow cracks, i.e., lower constraint conditions, are of interest. As discussed in Bergant et al. [17], the use of *P* vs. *CMOD* instead of *P* vs. *LLD* records is more suitable for estimating the *J*-integral values in specimens with shallow cracks and low constraint conditions.

Room temperature tests also allow the use of optical techniques in order to measure the stable crack growth as well as other fracture mechanics parameters as the *CTOD* or *CTOA*. Unlike the *J*-integral, these parameters are more empirical and present the advantage of having no theoretical limitations on their formulation and validity [27].

4.2. Material and anisotropy effects in *J*-resistance curves

In order to evaluate the material and anisotropy effects in fracture properties, the *J*-resistance curves of T1(T) and SE(T) "O" specimens at 300 °C are compared in Fig. 11. It can be seen that the curves for circumferential TWCs are higher than that for longitudinal TWCs for both materials. Moreover, the comparison between materials shows that the fracture toughness of Incoloy 800 SGTs is higher than for Inconel 690 SGTs both for circumferential and longitudinal TWCs. Similar findings can be obtained analyzing the *J*-resistance curves at room temperature.

Even when the SGTs under study are made of two different austenitic alloys, a possible reason that might explain the higher toughness observed for Incoloy 800 is its lower grain size (Fig. 1).

4.3. *J*-resistance curves validity limits

The necessary condition for the *J*-integral being a valid parameter to describe the stress and strain fields in the vicinity of a crack front is that the lengths of the crack, of the remaining ligament and the specimen's thickness are much larger than the crack tip opening displacement or *CTOD*. Given the equivalence between *J*-integral and *CTOD*, this limitation can be applied directly to the value of *J*.

In the case of SGTs fracture testing, wherein the specimen's thickness corresponds to the tube wall thickness, the validity condition for the *J*-integral can be related with the length of the initial remaining ligament b_0 , assuming a deep crack with $a/W = 0.5$ and $b_0 = a_0$.

In a similar manner, the validity condition for the *J*-integral

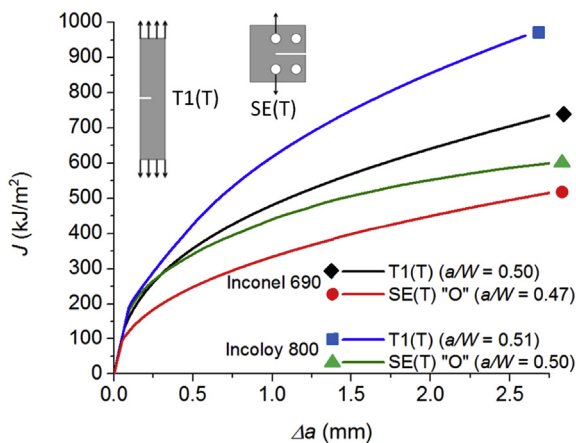


Fig. 11. Materials and anisotropy effects in *J*-resistance curves at 300 °C.

during stable crack growth is given if the elastic unloading zone, which size is about Δa , is small compared to b_0 .

The most common limits for *J*-resistance curves are defined in standard ASTM E1820-15 [25] as:

$$J_{\max} = \frac{b \sigma_f}{10} \quad (3)$$

$$\Delta a_{\max} = 0.25b_0 \quad (4)$$

where σ_f is the flow stress defined as $0.5(\sigma_{ys} + \sigma_u)$. Fig. 12 presents the most representative *J*-resistance curves with the inclusion of the limits J_{\max} and Δa_{\max} defined in Eqs. (3) and (4). It can be seen that the J_{\max} criterion is more limiting than Δa_{\max} , especially for curves obtained with circumferential TWCs. According to the criteria of ASTM E1820-15 [25], the curves are valid for stable crack growths lower than 1.5 mm approximately.

The J_{\max} condition results very limiting for austenitic materials, due to their relative low yield stress and high toughness. Schwalbe et al. [28] proposed to extend the validity of the *J*-integral for austenitic materials considering their great capacity for work hardening. For plane stress conditions, this new limit was considered to be given by Eq. (3) for bending loadings and doubling its value in the case of tensile loadings.

On the other hand, the above limitations have been formulated for standardized plane specimens, so its application to other conditions may not be appropriate.

An alternative way to study the validity of *J*-resistance curves obtained in this work is to compare the experimental *P* vs. *a/W* record corresponding to fracture testing with the corresponding plastic collapse loads P_{PC} for each specimen. These loads can be calculated from finite element numerical analyses applied to the different specimen geometries. Fig. 13 shows experimental records of *P* vs. *a/W* for all fracture tests performed at 300 °C compared with the results of the plastic collapse load P_{PC} vs. *a/W* obtained numerically. P_{PC} values were calculated using real stress vs. strain axial curves at 300 °C for both materials. Records for both SGTs materials were included in each figure.

It can be seen that the maximum loads achieved in the fracture tests are below the plastic collapse loads P_{CP} during all the stable crack growth stage. In the case of T1(T) specimens, Fig. 13(a), the experimental loads tend to approach the plastic collapse limit as stable crack growth develops. Eventually, the plastic collapse could be reached for longer crack growths. In this case, the stable crack

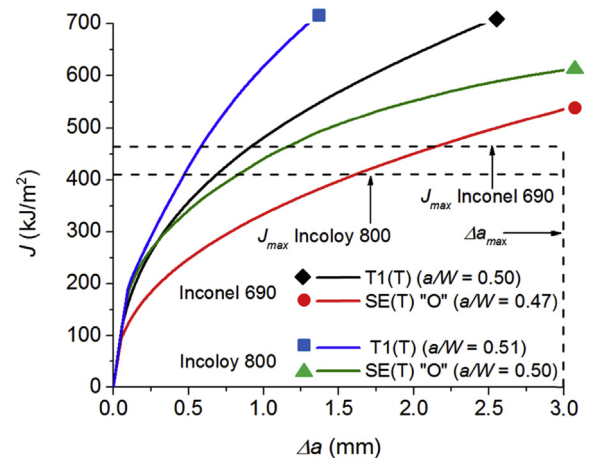


Fig. 12. J_{\max} and Δa_{\max} limits defined in ASTM E1820-15 [25] for *J*-resistance curves at 300 °C.

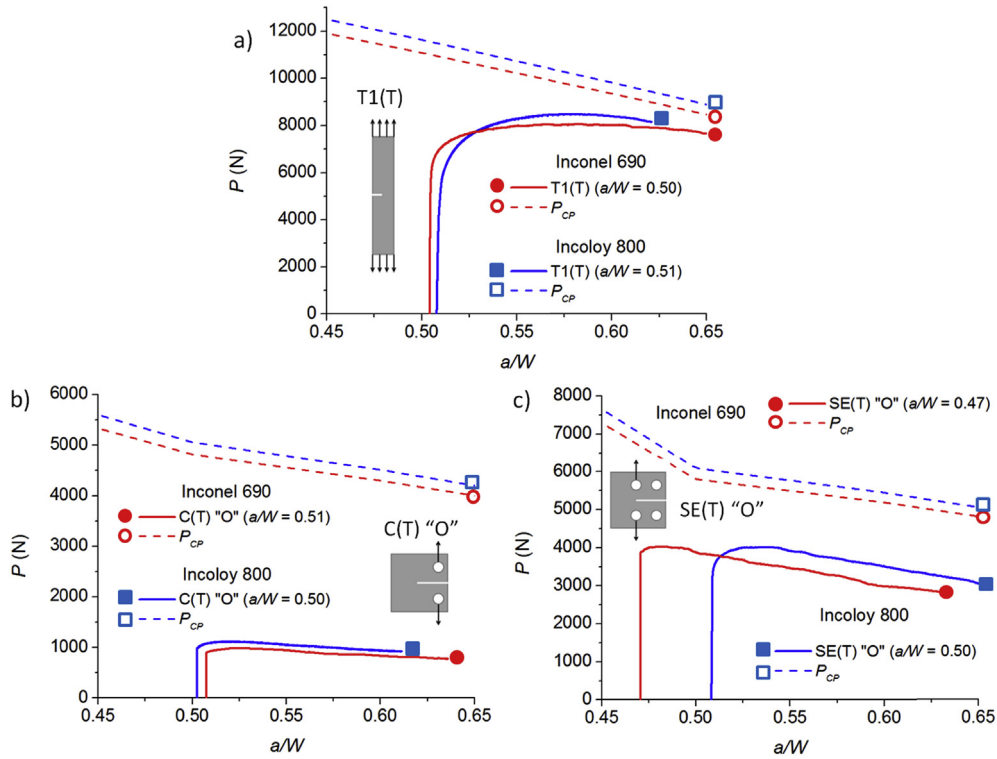


Fig. 13. Comparison of P vs. a/W experimental records and P_{CP} vs. a/W numerical results at 300 °C: (a) T1(T), (b) C(T) "O" and (c) SE(T) "O" specimens.

growth process would be controlled by a plastic collapse mechanism and the J -resistance curve would not be valid. For specimens with longitudinal TWCs, Fig. 13(b) and (c), the experimental loads remain considerably lower than P_{CP} limits and decrease more rapidly than P_{CP} loads as the crack grows. This behavior can be explained partially due to the lower fracture toughness presented by longitudinal TWCs regarding circumferential TWCs.

The analyses presented in Fig. 13 demonstrate that the stable crack growth process occurs through a ductile fracture mechanism at lower loading levels than the plastic collapse of the specimens. Assuming that the J -integral parameter controls this process, it would be possible to extend the validity of the J -resistance curves obtained in this work. A similar analysis can be performed in terms of J -integral values, comparing the experimental J -resistance curves with the numerical values of the applied J -integral for maximum loads, i.e., for P_{CP} . Even when the results lead to the same conclusion, the estimation of the J -integral for loads close to plastic collapse of the specimens may result imprecise. This is because the applied J -integral value can vary widely for small applied loads variations when a generalized plastic regime is achieved [29].

4.4. Comparison of results and summary of fracture properties

As mentioned previously, the references in open literature dealing with experimental data of fracture toughness of actual SGTs is very limited. Besides the previous works of the authors [16,18], two independent studies reported J -resistance curves for SGTs. Fig. 14 presents data published by Huh et al. [12] and Sanyal and Samal [19] together with some curves obtained in this work. All the J -resistance curves corresponded to tests performed at room temperature with the results not corrected due to stable crack growth.

Fig. 14(a) shows J -resistance curves for circumferential TWCs obtained with T1(T) specimens made of Inconel 600 [12], Inconel 690 and Incoloy 800 SGTs with ratios $a/W \sim 0.5$. It results clear that

the curve for Inconel 600 is quite higher than those obtained in this work. It should be noted that in the corresponding reference there is no mention about pre-cracking of the specimens, which could lead to higher load curves.

On the other hand, Fig. 14(b) shows a representative J -resistance curve obtained by Sanyal and Samal [19] using PL(T) (Pin-Loaded-Tension) specimens obtained from Incoloy 800 SGTs together with curves for C(T) "X" and SE(T) "X" specimens obtained in the present work. A very good agreement between these curves can be observed. This is especially noticeable in the case of PL(T) and C(T) "X" specimens. The last result can be understood taking into account that both specimens' configurations promote predominant bending loading conditions.

Table 3 summarizes the values of the fracture toughness parameter J_q . This single-parameter toughness value corresponds to the beginning of stable crack growth determined as the intersection between the experimentally determined J -resistance curves and a blunting line given by $J = 5 \sigma_f \Delta a$ and displaced 0.2 mm from the origin. The factor 5 in the blunting expression was estimated using the proposal of Landes [30] and the mechanical properties of Table 2. On the other hand, J_{1mm} is defined as the J -integral value after a stable crack growth of 1 mm following the recommendation of Wallin [31] who considered this single-parameter appropriate for characterizing ductile materials where the beginning of stable crack growth does not represent a critical condition. This definition is less dependent on the errors related to the crack growth measurement that are more likely to occur close to crack growth initiation [18] while it is independent on the blunting line expression used. For these reasons, J_{1mm} has been considered to represent a more consistent alternative to characterize the fracture toughness by means of a single-parameter [31].

J_{1mm} and J_q values presented in Table 3 demonstrate the high fracture toughness of SGTs materials.

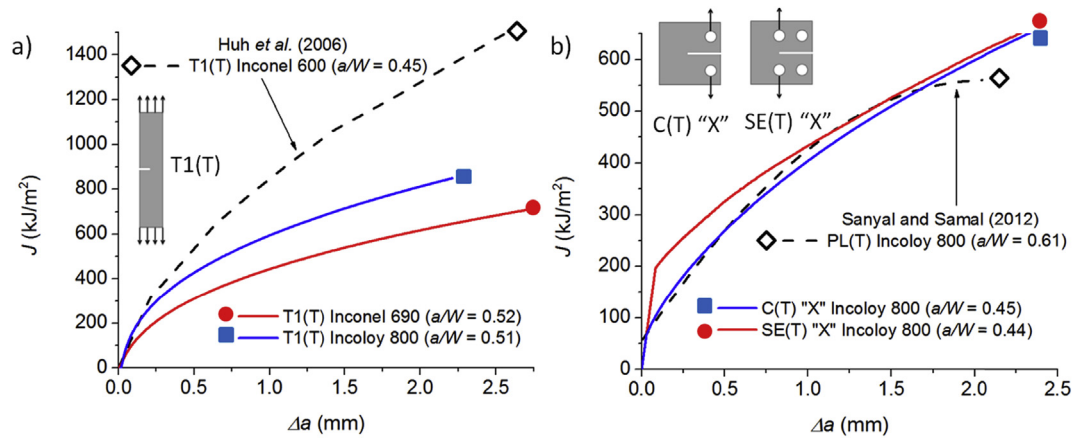


Fig. 14. Comparison of reported J -resistance curves for SGTs obtained in the present work with those published by Huh et al. [12] and Sanyal and Samal [19].

Table 3
Summary of fracture toughness properties for SGTs.

J_{1mm} (J_a) (kJ/m ²)	Inconel 690 ^a	Incoloy 800 ^b	Inconel 600 ^c	Incoloy 800 ^d
Circumferential TWCs	475 (303)	620 (365)	847 (525)	–
Longitudinal TWCs	334 (202)	455 (301)	–	424 (250)

^a T1(T) specimen at 300 °C.

^b SE(T) "O" specimen at 300 °C.

^c T1(T) specimen at room temperature [12].

^d PL(T) specimen at room temperature [19].

4.5. Potential role of environment and starter crack morphology on fracture toughness of SGTs

The fracture toughness properties reported in this work were obtained from specimens of service-unexposed material and from tests performed at room temperature and 300 °C in air environment, i.e., environmental conditions differing from the high temperature aqueous environment that the tubes experience in service. There is now growing experimental evidence showing that the fracture toughness of structural materials might be affected and eventually degraded by reactor coolant effects in reactor operating environments. For example, hydrogen generated from oxidation reactions could diffuse into the material changing the stacking-fault energy and thus affecting the plastic deformation behavior. However, the limited data existing in the open literature for austenitic stainless steels and nickel based alloys similar to that used in SGTs indicate that simulated nuclear environments have little, if any, effect on the fracture toughness properties [32,33]. On the other hand, the effects of thermal aging and environment on the fracture toughness of SGTs alloys have not reported so far. These considerations indicate the convenience of devoting further experimental efforts, seeking for a definitive elucidation of the matter. On the other hand, it is well known that cracks in SGTs developed in service conditions are initiated, primarily, by stress corrosion cracking (SCC) and have intergranular character [34–36]. Transgranular cracks originated from fatigue and also due to certain specific SCC mechanisms were also reported in some cases [1,20,34–36]. In the present work, the usual fracture mechanics practice of fatigue precracking was employed. This results in crack starters with a transgranular character. Although the effect of the starter crack morphology on fracture properties was not reported for SGTs alloys, some limited data for austenitic stainless steels show that using an intergranular crack starter instead of a transgranular fatigue crack had little or null effect on fracture toughness [32]. Related with this important aspect, it is worth mentioning

here the results of burst tests performed on SGTs removed from service and containing in-service induced SCC intergranular cracks and artificially machined crack-like defects [2]. The comparison of burst tests showed that the limit pressure does not depend on the sharpness of the cracks. This result can be understood taking into account that the fracture resistance curves of ductile materials are not sensitive to the crack sharpness, especially in the case of large levels of tearing [37,38]. As the critical event in the burst condition is achieved after some tearing of the tube wall, it can be assumed that the effect of the starter crack is reduced from the structural integrity perspective. Based on all the previous analysis, it can be considered that the J -resistance curves reported in the present work adequately represent the behavior of in-service cracked SGTs and thus can be used for structural assessments purposes.

5. Conclusions

The present study presented experimental results for J -resistance curves corresponding to two steam generator tubes (SGTs) made of Inconel 690 and Incoloy 800. Testing conditions included specimens with circumferential and longitudinal through-wall cracks (TWCs) in tensile predominant and bending predominant loadings in order to promote lower and higher constraint levels, respectively.

Tests were carried out at room temperature and 300 °C representing a typical operating condition for nuclear SGTs. It was found that the test temperature does not affect significantly the J -resistance curves obtained.

J -resistance curves for both circumferential and longitudinal TWCs were considerably higher for Incoloy 800 SGTs than those for Inconel 690 SGTs. Besides, for both materials, specimens with circumferential TWCs gave much higher resistance curves than longitudinal TWCs. These findings demonstrate high effects in fracture properties of SGTs due to the alloy considered (including its thermomechanical condition) and anisotropy.

Regarding the constraint levels in specimens promoted by tensile and bending loadings, a weak effect was found for deep cracks, i.e., $a/W \sim 0.5$. In general, tensile conditions and lower constraint levels lead to slightly higher J -resistance curves.

The validity limits for the J -resistance curves defined in ASTM E1820–15 [25] for standardized fracture specimens showed a very restrictive applicability of the curves obtained in this work. In order to extend this limiting condition, the experimental loads were compared with numerical plastic collapse loads for the specimens in consideration. It was found that stable crack growth during tests developed at much lower loads than those for plastic collapse. Therefore, the validity of the J -resistance curves obtained in this work can be extended considering that the J -integral parameter controls this fracture process. However, the J -resistance curves reported should be considered as specific to the SGT studied, i.e., are valid for the material and particular geometry of the tube.

Finally, J -resistance curves for SGTs reported by others authors were compared with the results obtained here. A good agreement was found between the curves for Incoloy 800 SGTs and longitudinal TWCs. On the other hand, curves reported for Inconel 600 SGTs with circumferential TWCs (T1(T) specimen) resulted considerably higher than those obtained in this work for Inconel 690 and Incoloy 800.

Acknowledgments

This work was supported by the Argentine National Atomic Energy Commission (Comisión Nacional de Energía Atómica, CNEA). The authors thank FAE SA (Ezeiza, Argentina) for the provision of SGTs used in this research.

References

- [1] IAEA-TECDOC-1668: Assessment and Management of Ageing of Major Nuclear Power Plant Components Important to Safety: Steam Generators, International Atomic Energy Agency, 2011.
- [2] B. Flesch, B. Cochet, Leak-before-break in steam generator tubes, *Int. J. Press. Vessel. Pip.* 43 (1990) 165–179, [http://dx.doi.org/10.1016/0308-0161\(90\)90099-4](http://dx.doi.org/10.1016/0308-0161(90)90099-4).
- [3] S. Majumdar, Prediction of structural integrity of steam generator tubes under severe accident conditions, *Nucl. Eng. Des.* 194 (1999a) 31–55, [http://dx.doi.org/10.1016/S0029-5493\(99\)00168-5](http://dx.doi.org/10.1016/S0029-5493(99)00168-5).
- [4] J. Lee, Y. Park, M. Song, Y. Kim, S. Moon, Determination of equivalent single crack based on coalescence criterion of collinear axial cracks, *Nucl. Eng. Des.* 205 (2001) 1–11, [http://dx.doi.org/10.1016/S0029-5493\(00\)00368-X](http://dx.doi.org/10.1016/S0029-5493(00)00368-X).
- [5] Z. Tonkovic, I. Skozrit, I. Alfirevic, Influence of flow stress choice on the plastic collapse estimation of axially cracked steam generator tubes, *Nucl. Eng. Des.* 238 (2008) 1762–1770, <http://dx.doi.org/10.1016/j.nucengdes.2008.01.008>.
- [6] L. Cizelj, B. Mavko, H. Riesch-Oppermann, A. Brucker-Froit, Propagation of stress corrosion cracks in steam generator tubes, *Int. J. Press. Vessel. Pip.* 63 (1995) 35–43, [http://dx.doi.org/10.1016/0308-0161\(94\)00046-L](http://dx.doi.org/10.1016/0308-0161(94)00046-L).
- [7] S. Majumdar, Failure and leakage through circumferential cracks in steam generator tubing during accident conditions, *Int. J. Press. Vessel. Pip.* 76 (1999b) 839–847, [http://dx.doi.org/10.1016/S0308-0161\(99\)00058-7](http://dx.doi.org/10.1016/S0308-0161(99)00058-7).
- [8] Y. Park, M. Song, J. Lee, S. Moon, Y. Kim, Investigation on the interaction effect of two parallel axial through-wall cracks existing in steam generator tube, *Nucl. Eng. Des.* 214 (2002) 13–23, [http://dx.doi.org/10.1016/S0029-5493\(02\)00010-9](http://dx.doi.org/10.1016/S0029-5493(02)00010-9).
- [9] X. Wang, W. Reinhardt, On the assessment of through-wall circumferential cracks in steam generator tubes with tube supports, *J. Press. Vessel Technol.* 125 (2003) 85–90, <http://dx.doi.org/10.1115/1.1511737>.
- [10] Z. Tonkovic, I. Skozrit, J. Soric, A contribution to assessment of steam generator tubes integrity, in: 11th International Conference on Fracture, 01/2005, 4, 2005 (Turin, Italy).
- [11] Y. Chang, Y. Kim, S. Hwang, J. Kim, Burst pressure estimation of steam generator tubes based on fracture mechanics analyses, *Key Eng. Mater.* 321–323 (2006) 666–669, <http://dx.doi.org/10.4028/www.scientific.net/KEM.321-323.666>.
- [12] N. Huh, J. Kim, Y. Chang, Y. Kim, S. Hwang, J. Kim, Elastic-plastic fracture mechanics assessment for steam generator tubes with through-wall cracks, *Fatigue & Fract. Eng. Mater. Struct.* 30 (2006) 131–142, <http://dx.doi.org/10.1111/j.1460-2695.2006.01094.x>.
- [13] J. Hu, F. Liu, G. Cheng, Z. Zhang, Determination of the critical crack length for steam generator tubing based on fracture-mechanics-based method, *Ann. Nucl. Energy* 38 (2011) 1900–1905, <http://dx.doi.org/10.1016/j.anucene.2011.05.009>.
- [14] M. Bergant, A. Yawny, J. Perez Ipiña, Failure assessment diagram in structural integrity analysis of steam generator tubes, *Procedia Mater. Sci.* 8 (2015a) 128–138, <http://dx.doi.org/10.1016/j.mspro.2015.04.056>.
- [15] M. Bergant, A. Yawny, J. Perez Ipiña, Structural integrity assessments of steam generator tubes using the FAD methodology, *Nucl. Eng. Des.* 295 (2015b) 457–467, <http://dx.doi.org/10.1016/j.nucengdes.2015.09.022>.
- [16] M. Bergant, A. Yawny, J. Perez Ipiña, Estimation procedure of J -resistance curves for through wall cracked steam generator tubes, *Procedia Mater. Sci.* 1 (2012) 273–280, <http://dx.doi.org/10.1016/j.mspro.2012.06.037>.
- [17] M. Bergant, A. Yawny, J. Perez Ipiña, Numerical study of the applicability of the η -factor method to J -resistance curve determination of steam generator tubes using non-standard specimens, *Eng. Fract. Mech.* 146 (2015c) 109–120, <http://dx.doi.org/10.1016/j.engfractmech.2015.07.059>.
- [18] M. Bergant, A. Yawny, J. Perez Ipiña, Experimental determination of J -resistance curves of nuclear steam generator tubes, *Eng. Fract. Mech.* 164 (2016) 1–18, <http://dx.doi.org/10.1016/j.engfractmech.2016.07.008>.
- [19] G. Sanyal, M. Samal, Assessment of axial cracking of a steam generator tube, *J. Metall. Eng.* 1 (2012) 53–62.
- [20] EPRI, Steam Generator Integrity Assessment Guidelines. Revision 2, 2006. Technical Report 1012987.
- [21] ASTM A370–12 standard test methods and definitions for mechanical testing of steel products, *Am. Soc. Test. Mater.* (2012), <http://dx.doi.org/10.1520/A0370-12>.
- [22] J. Rice, P. Paris, J. Merkle, Some further results of J -integral analysis and estimates. Progress in flaw growth and fracture toughness testing, *ASTM STP* 536 (1973) 231–245, <http://dx.doi.org/10.1520/STP496435>.
- [23] M. Bergant, Evaluación de tenacidad a la fractura e integridad estructural de tubos de generadores de vapor nucleares, Doctoral thesis, Instituto Balseiro, Universidad Nacional de Cuyo – CNEA, Argentina, 2016.
- [24] H.A. Ernst, P.C. Paris, J.D. Landes, Estimations on J -integral and tearing modulus T from a single specimen test record. Fracture mechanics: thirteenth conference, *ASTM STP* 743 (1981) 476–502, <http://dx.doi.org/10.1520/STP288145>.
- [25] ASTM E1820–15 standard test method for measurement of fracture toughness, *Am. Soc. Test. Mater.* (2015), <http://dx.doi.org/10.1520/E1820-15>.
- [26] ASME Boiler and Pressure Vessel Code, Section II, Part D, American Society of Mechanical Engineers, 2010.
- [27] J. Perez Ipiña, *Mecánica de Fractura*, Librería y Editorial Alsina, Buenos Aires, Argentina, 2004.
- [28] K.H. Schwalbe, A. Cornec, K. Baustian, Application of fracture mechanics principles to austenitic steels, *Int. J. Press. Vessel. Pip.* 65 (1996) 193–207, [http://dx.doi.org/10.1016/0308-0161\(96\)00131-5](http://dx.doi.org/10.1016/0308-0161(96)00131-5).
- [29] T. Anderson, *Fracture Mechanics, Fundamentals and Applications*, CRC Press, Boca Raton, Florida, 2005.
- [30] J.D. Landes, The blunting line in elastic-plastic fracture, *Fatigue Fract. Eng. Mater. Struct.* 18 (1995) 1289–1297, <http://dx.doi.org/10.1111/j.1460-2695.1995.tb00855.x>.
- [31] K. Wallin, *Fracture Toughness of Engineering Materials, Estimation and Application*, EMAS Publishing, Warrington, UK, 2011.
- [32] C.M. Brown, W.J. Mills, Effect of water on mechanical properties and stress corrosion behavior of Alloy 600, Alloy 690, EN82H Welds, and EN52 Welds, *Corrosion* 55 (2) (1999) 173–186, <http://dx.doi.org/10.5006/1.3283978>.
- [33] NUREG/CR-6960, Crack Growth Rates and Fracture Toughness of Irradiated Austenitic Stainless Steels in BWR Environments, United States Nuclear Regulatory Commission, Office of Nuclear Regulatory Research, 2008.
- [34] R.W. Staehle, J.A. Gorman, Quantitative assessment of submodes of stress corrosion cracking on the secondary side of Steam Generator Tubing in Pressurized Water Reactors: part 1, *Corrosion* 59 (11) (2003) 931–994, <http://dx.doi.org/10.5006/1.3277522>.
- [35] R.W. Staehle, J.A. Gorman, Quantitative assessment of submodes of stress corrosion cracking on the secondary side of Steam Generator Tubing in Pressurized Water Reactors: part 2, *Corrosion* 60 (1) (2004) 5–63, <http://dx.doi.org/10.5006/1.3299232>.
- [36] R.W. Staehle, J.A. Gorman, Quantitative assessment of submodes of stress corrosion cracking on the secondary side of Steam Generator Tubing in Pressurized Water Reactors: part 3, *Corrosion* 60 (2) (2004) 115–180, <http://dx.doi.org/10.5006/1.3287716>.
- [37] G.M. Spink, P.J. Worthington, P.T. Heald, The effect of notch acuity on fracture toughness testing, *Mater. Sci. Eng.* 11 (1973) 113–117, [http://dx.doi.org/10.1016/0025-5416\(73\)90051-7](http://dx.doi.org/10.1016/0025-5416(73)90051-7).
- [38] P. Moore, The effect of notch sharpness on the fracture toughness determined from SENT specimens, in: Proceedings of the ASME 2014 33rd International Conference on Ocean, Offshore and Arctic Engineering, Vol. 5, 2014, <http://dx.doi.org/10.1115/OMAE2014-24663>. San Francisco, California, U. S. A.